Article

Intramolecular sp^2-sp^3 Disequalization of Chemically Identical Sulfonamide Nitrogen Atoms: Single Crystal X-Ray Diffraction Characterization, Hirshfeld Surface Analysis and DFT Calculations of *N*-Substituted Hexahydro-1,3,5-Triazines

Alexey V. Kletskov [1] , **Diego M. Gil** [2] , **Antonio Frontera** [3,*] , **Vladimir P. Zaytsev** [1] ,
Natalia L. Merkulova [1] , **Ksenia R. Beltsova** [1] , **Anna A. Sinelshchikova** [4] , **Mikhail S. Grigoriev** [4] ,
Mariya V. Grudova [1] and **Fedor I. Zubkov** [1,*]

[1] Organic Chemistry Department, Faculty of Science, Peoples' Friendship University of Russia (RUDN University), 6 Miklukho-Maklaya St., Moscow 117198, Russia; avkletskov@gmail.com (A.V.K.); vzaitsev@sci.pfu.edu.ru (V.P.Z.); fraumerk@gmail.com (N.L.M.); k.beltsova17@mail.ru (K.R.B.); shokoi@mail.ru (M.V.G.)

[2] INBIOFAL (CONICET-UNT), Instituto de Química Orgánica-Cátedra de Química Orgánica I, Facultad de Bioquímica, Química y Farmacia, Universidad Nacional de Tucumán, Ayacucho 471, San Miguel de Tucumán, Tucumán T4000INI, Argentina; diegomauriciogil@gmail.com

[3] Department de Química, Universitat de les Illes Balears, Crta de Valldemossa km 7.5, 07122 Palma de Mallorca (Baleares), Spain

[4] Frumkin Institute of Physical Chemistry and Electrochemistry, Russian Academy of Sciences, Leninsky pr. 31, bld. 4, Moscow 119071, Russia; asinelshchikova@gmail.com (A.A.S.); mickgrig@mail.ru (M.S.G.)

* Correspondence: toni.frontera@uib.es (A.F.); fzubkov@sci.pfu.edu.ru (F.I.Z.)

check for updates

Abstract: In this manuscript, the synthesis and single crystal X-ray diffraction characterization of four N-substituted 1,3,5-triazinanes are reported along with a detailed analysis of the noncovalent interactions observed in the solid state architecture to these compounds, focusing on C–H···π and C–H···O H-bonding interactions. These noncovalent contacts have been characterized energetically by using DFT calculations and also by Hirshfeld surface analysis. In addition, the supramolecular assemblies have been characterized using the quantum theory of "atoms-in-molecules" (QTAIM) and molecular electrostatic potential (MEP) calculations. The XRD analysis revealed a never before observed feature of the crystalline structure of some molecules: symmetrically substituted 1,3,5-triazacyclohexanes possess two chemically identical sulfonamide nitrogen atoms in different sp^2 and sp^3-hybridizations.

1. Introduction

N-substituted triazinanes are interesting molecules that are used as efficient aminomethylation reagents and as formal 1,4- and 1,2-dipolar adducts in annulation reactions [1–10]. Moreover, this type of molecules presents remarkable antimicrobial activity [11]. While the access to symmetric N-substituted triazinanes is simple, there was no convenient method for the synthesis of triazinanes bearing different substituents on nitrogen atoms. Recently, we have described a straightforward

approach to *N*-alkyl-*N'*,*N''*-substituted triazinanes that is based on a one-pot multi-component reaction of amines, paraformaldehyde and sulfonamides or thioureas [12].

In this manuscript, the synthesis, single crystal X-ray diffraction characterization, Hirshfeld surface analysis and density functional theory (DFT) calculations of four triazinanes (see Scheme 1) are reported. The combination in the same structure of butyl substituents (*n*-Bu or *t*-Bu) with two aromatic rings facilitates the formation of a variety of C–H···π interactions in combination with C–H···O/N bonds. These noncovalent interactions have been studied using Hirshfeld surface analysis and DFT calculations. Moreover, they have been rationalized using the quantum theory of atoms in molecules (QTAIM) and molecular electrostatic potential (MEP) surfaces.


1: R = Me;
2: R = H

3: R = Me;
4: R = H
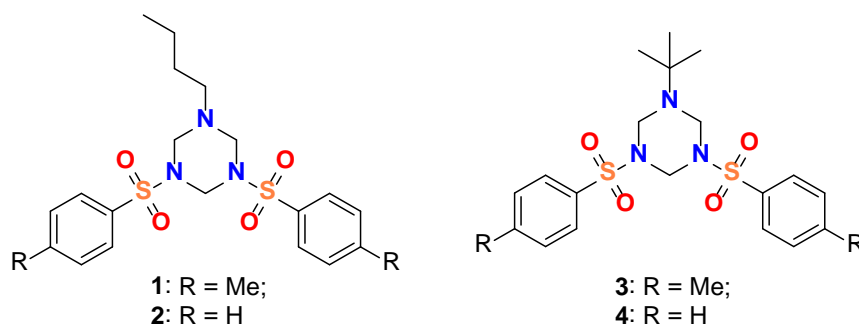
Scheme 1. Compounds **1**–**4** studied in this work.

2. Materials and Methods

2.1. Experimental Details

As it was mentioned above, the main objects of this work, *N*,*N'*-disulfamide substituted triazinanes **1**–**4**, were prepared according to the method described in our preliminary communication [12] using the three-component Mg(ClO₄)₂ catalyzed condensation of arylsulfonamides with paraformaldehyde and *n*- or *tert*-butyl amine (Scheme 2, see the Supplementary Materials for detail of the experimental procedures and spectral data). The *tert*-butyl- and *n*-butylamines were chosen as the amino-components providing the highest yield of the target triazinanes.

Alkyl = *n*-Bu, *t*-Bu; Ar = Ph, 4-MeC₆H₄
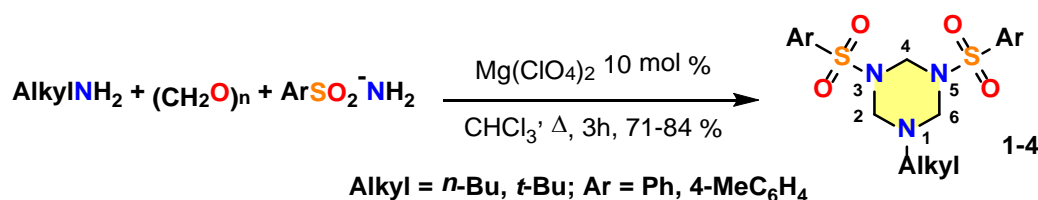
Scheme 2. Synthesis of 1,3,5-triazacyclohexanes **1**–**4**.

All obtained triazinanes are well-crystallized solids that allowed the growth of crystals suitable for XRD analysis.

2.2. Crystallographic Details

Single crystal X-ray diffraction experiments were performed at the Center for Shared Use of Physical Methods of Investigation at the Frumkin Institute of Physical Chemistry and Electrochemistry. The single crystal X-ray diffraction data for 1,3,5-triazacyclohexanes (**1**–**4**) were collected on a Bruker Kappa Apex II automatic four-circle diffractometer (Bruker AXS, Madison, WI, USA) equipped with an area detector (Mo-Kα sealed-tube X-ray source, λ = 0.71073 Å, graphite monochromator) at 100 K for all compounds. The principal crystallographic data and structural refinements are summarized in Table 1. Atomic coordinates for compounds **1**–**4**, have been deposited with the CCDC

(number 1992667–1992670). The supplementary crystallographic data are available in the ESI section. The comparison of the crystal structure parameters with the analogous compounds were performed using ConQuest search in Cambridge Structural Database (CSD, Version 5.40). The histograms of angles values were obtained from a graphical search of sulfonamides ($C–S(=O)_2–NC_2$) with 3D parameters for angles. More than 7000 hits were analyzed.

Table 1. Crystal data and structure refinement for **1–4**.

Identification Code	1	2	3	4
CCDC number	1992667	1992668	1992669	1992670
Empirical formula	$C_{21}H_{29}N_3O_4S_2$	$C_{19}H_{25}N_3O_4S_2$	$C_{21}H_{29}N_3O_4S_2$	$C_{19}H_{25}N_3O_4S_2$
Formula weight	451.59	423.54	451.59	423.54
Temperature/K	100(2)	100(2)	100(2)	100(2)
Crystal system	monoclinic	monoclinic	monoclinic	orthorhombic
Space group	$P2_1/c$	$P2_1/n$	$P2_1/n$	$P2_12_12_1$
a/Å	13.2871(4)	8.4284(2)	5.955(4)	10.7298(3)
b/Å	10.3261(3)	25.9248(8)	15.378(12)	11.1010(3)
c/Å	15.9595(4)	9.5601(3)	23.915(19)	16.9303(5)
α/°	90	90	90	90
β/°	90.511(2)	106.639(1)	90.968(16)	90
γ/°	90	90	90	90
Volume/Å^3	2189.62(11)	2001.46(10)	2190(3)	2016.59(10)
Z	4	4	4	4
ρ_{calc}g/cm^3	1.370	1.406	1.370	1.395
μ/mm^{-1}	0.276	0.297	0.276	0.295
F(000)	960.0	896.0	960.0	896.0
Crystal size/mm^3	0.440 × 0.360 × 0.320	0.400 × 0.320 × 0.260	0.500 ×0.180 × 0.030	0.420 × 0.400 × 0.360
Radiation	MoKα (λ = 0.71073)	MoKα (λ = 0.71073)	MoKα (λ = 0.71073)	MoKα (λ = 0.71073)
2Θ range for data collection/°	7.126 to 59.998	7.392 to 59.994	8.476 to 55	8.16 to 69.998
Index ranges	$-18 \leq h \leq 18, -14 \leq k \leq 14, -20 \leq l \leq 22$	$-6 \leq h \leq 11, -35 \leq k \leq 36, -13 \leq l \leq 13$	$-4 \leq h \leq 7, -19 \leq k \leq 19, -31 \leq l \leq 31$	$-17 \leq h \leq 16, -17 \leq k \leq 16, -19 \leq l \leq 27$
Reflections collected	33914	28404	14104	35553
Independent reflections	6383 [R_{int} = 0.0390, R_{sigma} = 0.0303]	5835 [R_{int} = 0.0351, R_{sigma} = 0.0280]	4940 [R_{int} = 0.1432, R_{sigma} = 0.1883]	8855 [R_{int} = 0.0303, R_{sigma} = 0.0303]
Data/restraints/parameters	6383/0/273	5835/0/253	4940/6/274	8855/0/253
Goodness-of-fit on F^2	1.029	1.035	1.049	1.042
Final R indexes [I >= 2σ (I)]	R_1 = 0.0350, wR_2 = 0.0877	R_1 = 0.0334, wR_2 = 0.0824	R_1 = 0.1398, wR_2 = 0.3472	R_1 = 0.0283, wR_2 = 0.0698
Final R indexes [all data]	R_1 = 0.0457, wR_2 = 0.0939	R_1 = 0.0423, wR_2 = 0.0873	R_1 = 0.2253, wR_2 = 0.4075	R_1 = 0.0316, wR_2 = 0.0715
Largest diff. peak/hole/e Å^{-3}	0.38/−0.37	0.39/−0.37	0.94/−0.55	0.36/−0.28

2.3. Hirshfeld Surface Calculations

The Hirshfeld surface (HS) analysis [13–15] and their associated 2D fingerprint plots (full and decomposed) [16] were carried out employing the CrystalExplorer 17 program [17] in order to visualize and quantify various non-covalent interactions that stabilize the crystal packing. The HS was mapped over d_{norm} property. The d_{norm} property is a symmetric function of distances to the surface from nuclei inside and outside the Hirshfeld surface (di and de, respectively), relative to their respective van der Waals radii. The regions with red and blue color on the d_{norm} represent the shorter and longer inter contacts while the white color indicates the contacts around the van der Waals radii. 2D fingerprint plots provide relevant information of intermolecular contacts in the crystal. The d_{norm} surface was mapped with the color scale in the range −0.050 au (red) to 0.600 au (blue). 2D fingerprint plots (di vs. de) were displayed using the expanded 0.6–2.8 Å range.

2.4. Theoretical Methods

All DFT calculations were carried out using the Gaussian-16 program [18] at the PBE1PBE-D3/def2-TZVP level of theory and using the crystallographic coordinates. The formation energies of the assemblies were evaluated by calculating the difference between the total energy of the assembly and the sum of the monomers that constitute the assembly, which have been maintained frozen. That is $\Delta E_{AB} = E_{AB} − E_A − E_B$, where ΔE_{AB} is the interaction energy; E_{AB} is the energy of the dimer and E_A and E_B are the energy of the monomers. The BSSE has been used to correct the interaction energies by using the counterpoise =2 keyword in the Gaussian-19 program [18]. The molecular electrostatic potential was computed at the same level of theory and plotted onto the 0.001 a.u. isosurface. The Quantum Theory of Atoms-in-Molecules (QTAIM) [19] analysis was carried

out at the same level of theory by means of the AIMAll program [20] to obtain the distribution of bond critical points (CPs) and bond paths [21].

3. Results

3.1. Structural Description

According to the single crystal X-ray diffraction data, molecules **1**–**4** comprise the 1,3,5-triazacyclohexane ring bearing three substituents at the nitrogen atoms (see Figure 1).
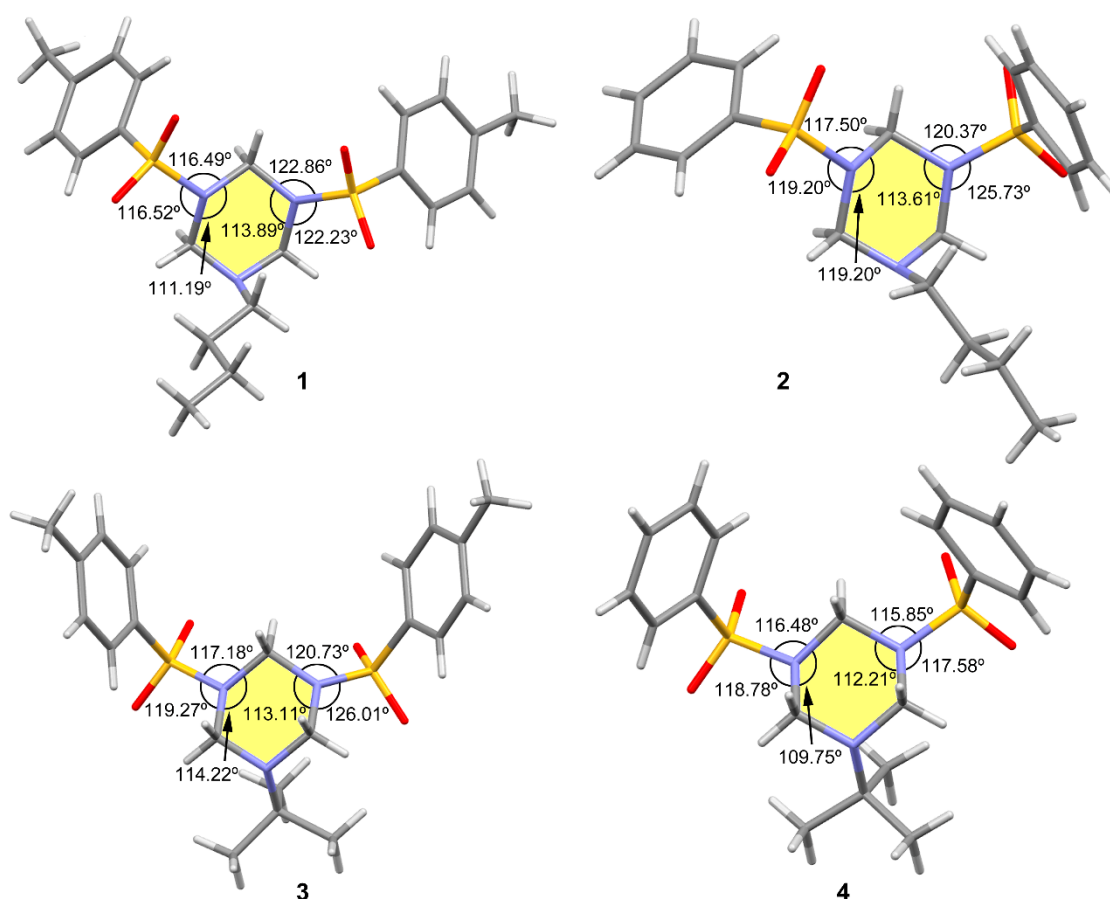

Figure 1. Single crystal X-ray diffraction structures of triazinanes **1**–**4**.

The asymmetric unit contains one molecule of each triazine. The general geometrical features of these systems are similar, which are the slightly distorted chair conformation of the six-membered ring, with the *N*-alkyl substituents (*n*-Bu or *t*-Bu) occupying the axial position and the two *N*-sulfamide fragments occupying the sterically favorable pseudo-equatorial orientation (see Table S2 for torsion angles of *N*-substituents). The atoms C2, C6, N3, and N5 of the triazinane cycle in all structures lie nearly in one plane (the deviation of one atom from the plane of the other three is less than 0.03 Å), while the deviation of N1 and C4 atoms from this plane range from −0.633(2) Å to −0.661(2) Å and from 0.643(14) Å to 0.712(2) Å, correspondingly, therefore the molecules have a classical chair-conformation of the central heterocycle (see Scheme 2 for atom numbering scheme). All CH$_2$-N bond lengths and CH$_2$–N–CH$_2$ bond angles are typical for 1,3,5-triazinanes and are listed in the corresponding tables in (Supplementary Materials Table S2–S15). The torsion angles CNCN in the triazacyclohexane ring are close to 60° (see Table S2).

The most intriguing and distinguishing feature of the triazinanes under discussion is the unprecedented geometry of the N3 and N5 nitrogen atoms of the sulfonamide fragments in the

N-butyl substituted heterocycles **1** and **2**. As is generally known, the nitrogen atom in a sulfonamide group can adopt both sp^2 and sp^3 hybridization depending on substituents at the nitrogen atom [22–24]. However, according to the data of the CCDC, there are no known examples of 1,3,5-triazinanes or other saturated six-membered azaheterocycles simultaneously possessing two chemically identical sulfonamide nitrogen atoms in different hybridization. Analysis of the values of the sums of valence angles at nitrogen atoms in positions 3 and 5 allows to clearly identify atoms in sp^2 or in sp^3 hybridization (Figure 1 and Table 2). The N3-atoms in compounds **1–3** are sp^2-hybridizated and, as a result, they assume the flat trigonal configuration (the sum of the angles is close to 360°). N5-Atoms, chemically equivalent to N3-atoms, in the same molecules adopt the tetrahedral configuration (the sum of the angles lies in the diapason of 344–351°) and, therefore, are sp^3-hybridizated. This is most clearly seen in the examples of compounds **1** and **2**. The presence of the *tert*-butyl group at the N1 position in compounds **3** and **4**, probably due to its high steric volume, symmetrizes the molecules, leveling the difference between both sulfonamide nitrogen atoms in a crystal. This is also observed in the equalization of the S–N distances of the sulfonamide groups in compounds **3** and **4** compared to **1** and **2**, see Table 2. The largest difference between both S–N distances is observed in compound **2**, i.e., 0.016 Å. In fact, the short S2–N5 distance is an indication of a partial double bond character, in agreement with the sp^2-hybridization.

Table 2. Sums of angles at the sulfonamide nitrogen atoms N3 and N5 and S–N distances in 1,3,5-triazinanes **1–4**.

Compound	1	2	3	4
Alkyl	Bu	Bu	*t*-Bu	*t*-Bu
SO$_2$Ar	SO$_2$C$_6$H$_4$Me	SO$_2$Ph	SO$_2$C$_6$H$_4$Me	SO$_2$Ph
Sum of angles around N3 (°)	359.0	359.7	359.8	345.0
Sum of angles around N5 (°)	344.2	347.4	350.7	345.6
S1–N3 distance (Å)	1.642(1)	1.630(1)	1.632(9)	1.640(1)
S2–N5 distance (Å)	1.632(1)	1.614(1)	1.629(9)	1.638(1)

Compound **1** crystallizes in the monoclinic crystal system in the space group $P2_1/c$. Selected bond lengths, angles and torsional angles are shown in Tables S2–S5. The S2–C21 and S1–N3 bond lengths of 1.758(1) and 1.642(1) Å respectively are in agreement with a single bond character of these bonds [24]. The S–O bond distances of the sulfamide moiety are in the range 1.432(1)–1.436(1) Å, which is typical for *N*-sulfamides. The SO$_2$ group has typical angles if compare with CSD data for N-sulfamides (Figure S1 in Supplementary Materials): O–S–O angle is around 120° [O1–S1–O2 is 119.95(6)°], while N–S–O angles are between 105° and 115° [N3–S1–O2 is 106.07(6)°, N3–S1–O1 is 106.63(5)°].

The crystal structure of this compound exhibits interesting assemblies in the solid state (see Table S3 for H-bonds). For instance, Figure 2a shows a self-assembled dimer dominated by C–H···O interactions where the methyl group in para acts as a H-bond donor. The acidity of these protons is higher than usual for a methyl group due to the presence of the electron withdrawing sulfamide group. Quite remarkable is the ternary assembly shown in Figure 2b, where the aromatic π-cloud interacts simultaneously with the methyl group at one side and an aromatic C–H bond at the opposite side, thus forming a C–H···π···H–C assembly. It is worth noting that the C–H···π distances are very short (2.60 and 2.70 Å) thus, confirming their relevance in the solid state of this compound.

Compound **2** crystallizes in the monoclinic crystal system in the space group $P2_1/n$ and the main difference with compound **1** is the absence of methyl groups. In addition, the sulfonamide groups are attached to the 1,3,5-triazacyclohexane ring in different orientations as reflected by the C6–N5–S2–C21 and C2–N3–S1–C11 torsional angles of −105.0(1)° and −65.5(1)°, respectively. It also forms self-assembled dimers in the solid state, where both C–H···π and C–H···O (Table S3) interactions are established, as shown in Figure 3a. Moreover, it also forms infinite 1D supramolecular chains in

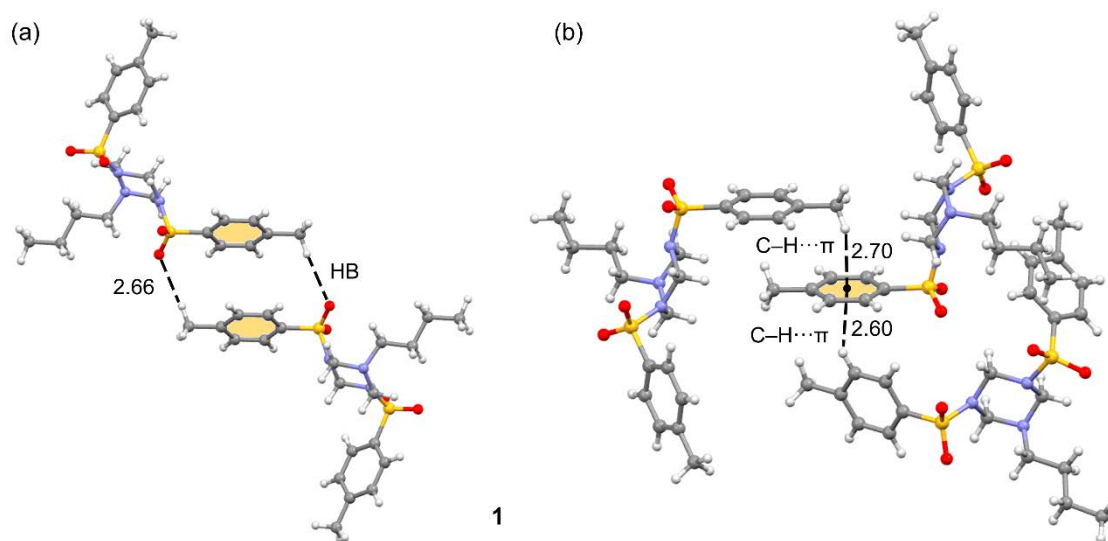the solid state promoted by C–H···O interactions involving the butyl chain and the sulfonamide group (see Figure 3b).

Figure 2. (**a**) Self assembled dimer in compound **1**. (**b**) C–H···π···H–C assembly in the solid state of structure **1**. Distances in Å. For the C–H···π interactions, the distances are measured from the H-atom to the ring centroid.
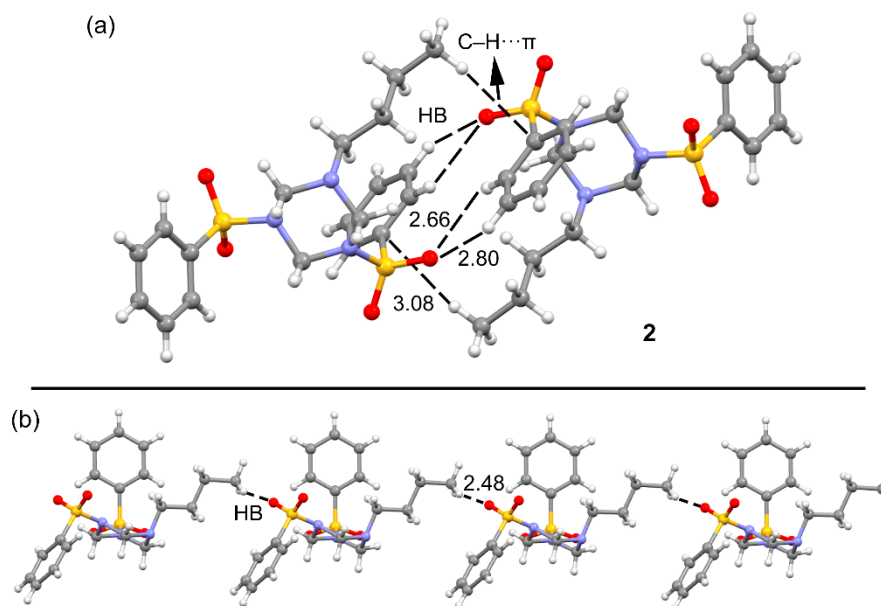

Figure 3. (**a**) Self-assembled dimer of compound **2**. (**b**) 1D supramolecular chain in **2**. Distances in Å. The C–H···π interaction distances are measured from the H-atom to the closest C-atom of the ring.

Compound **3** crystalizes in the monoclinic crystal system in the space group $P2_1/n$ and, similarly to compound **1**, also forms ternary assemblies where the same aromatic ring establishes C–H···π interactions at both sides of the ring, thus forming a C–H···π···H–C assembly (see Figure 4). This compound also forms 1D supramolecular chains in the solid state where the H-atoms of the triazinane ring interact with the O-atoms of the sulfonamide groups (Table S3), as shown in Figure 4b. The formation of this assembly is facilitated by the relative orientation of the *p*-methyl-benzene-sulfonamide groups.

(a)　　　　　　　　　　　　　　　　　　　　(b)
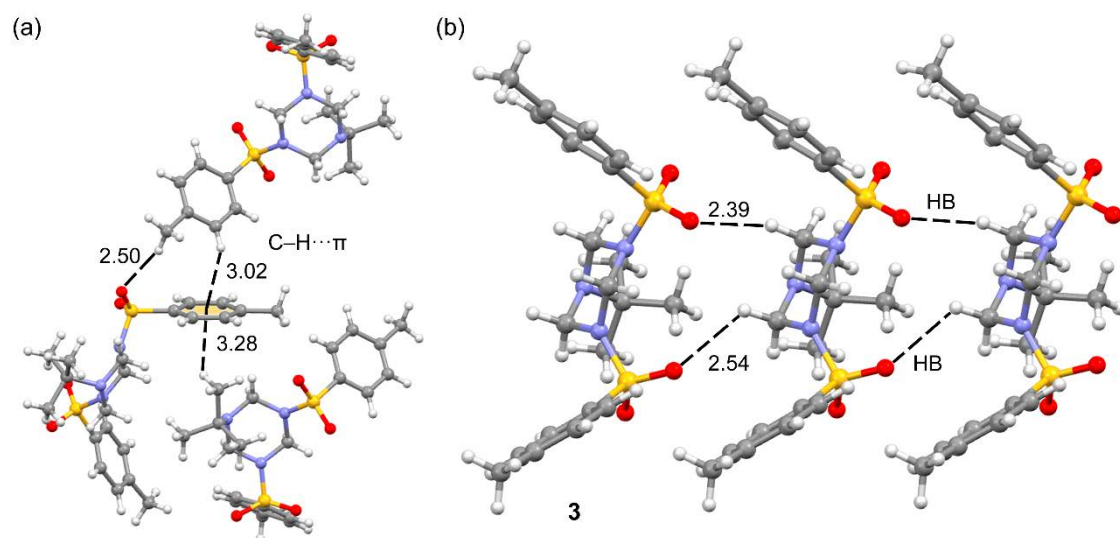
Figure 4. (**a**) C–H···π···H–C assembly in the solid state of structure **3**. Distances in Å. (**b**) 1D supramolecular chain in **3**. Distances in Å. For the C–H···π interactions, the distances are measured from the H-atom to the ring centroid.

Compound **4** crystallizes in the orthorhombic crystal system in the space group $P2_12_12_1$ and also exhibits several motifs in the solid state that are mainly dominated by C–H···O interactions (Table S3). As examples, two motifs are given in Figure 5, one corresponds to a discrete dimer where three H-bonds are formed and the other one to a 1D supramolecular polymer also governed by the formation of C–H···O bonds involving the aromatic H-atom located in para to the sulfonamide group (Figure 5b).

(a)

(b)
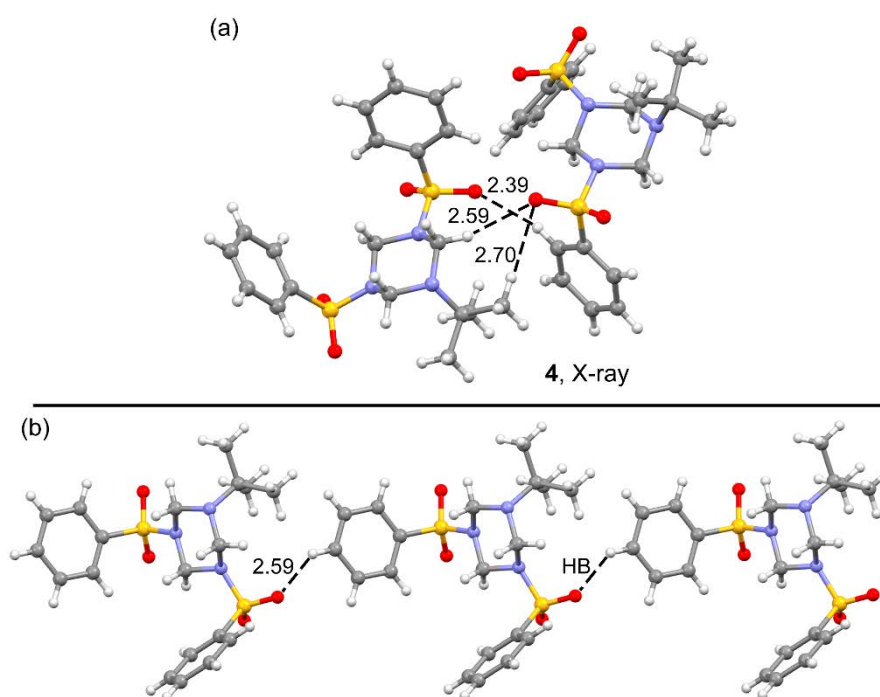
Figure 5. (**a**) Self-assembled dimer of compound **4**. (**b**) 1D supramolecular chain in **4**. Distances in Å.

3.2. Hirshfeld Surfaces

The Hirshfeld surface analysis is a very convenient tool for analyzing intermolecular interactions. The HS surfaces mapped over d_{norm} property are displayed in Figure 6 highlighting the main intermolecular interactions and scheme of labels. The patterns of intermolecular interactions are similar in all structures, which prompted us to evaluate the contributions of the weak non-covalent contacts in the supramolecular assembly, as well as the importance of C–H···π interactions in stabilization of the crystal packing. The 2D fingerprint plots (Figure 7) of the molecules illustrate significant differences between the intermolecular interaction patterns. The surfaces are shown as transparent to allow the visualization of the molecules. Contacts with distances equal to the sum of van der Waals (vdW) radii are represented as white regions and contacts with distances shorter than and longer than the vdW radii are shown as red and blue colors, respectively.
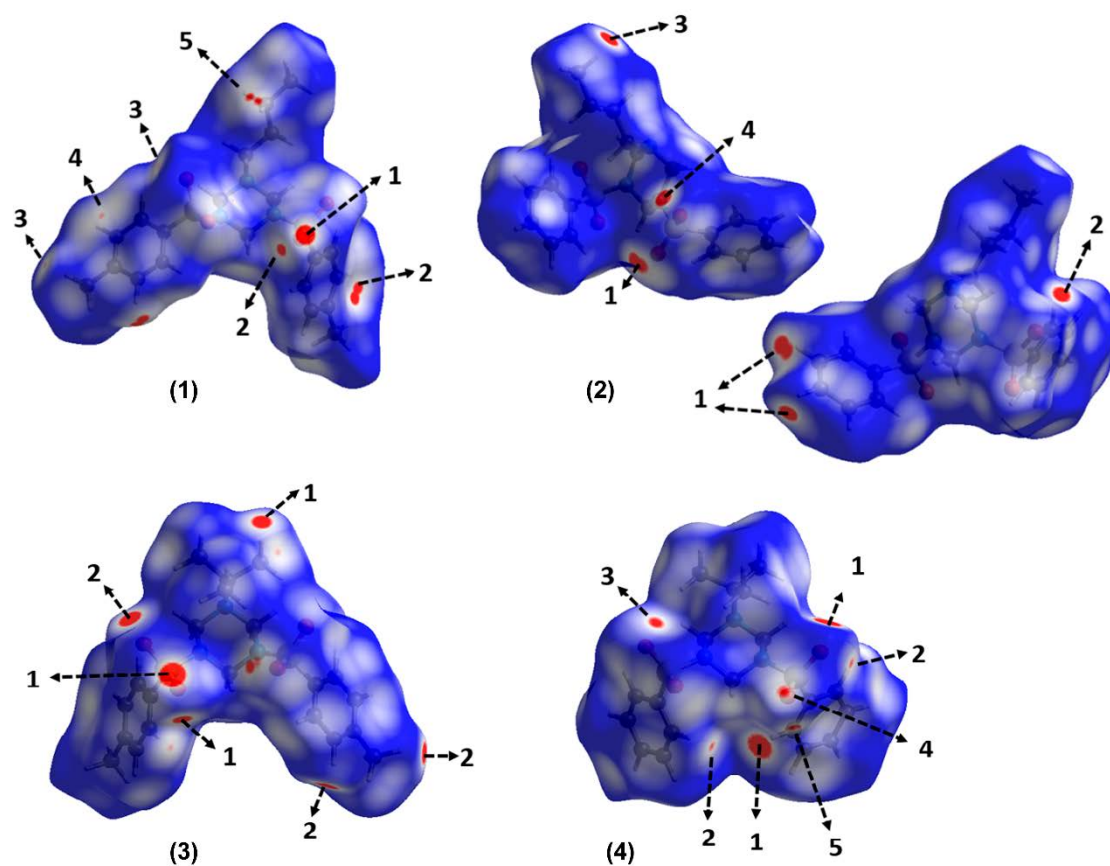
Figure 6. Hirshfeld surfaces mapped over d_{norm} function for compounds **1–4**. The labels are discussed in the text. For compound (**2**), the second molecule is rotated by 180° around the vertical axis of the plot.
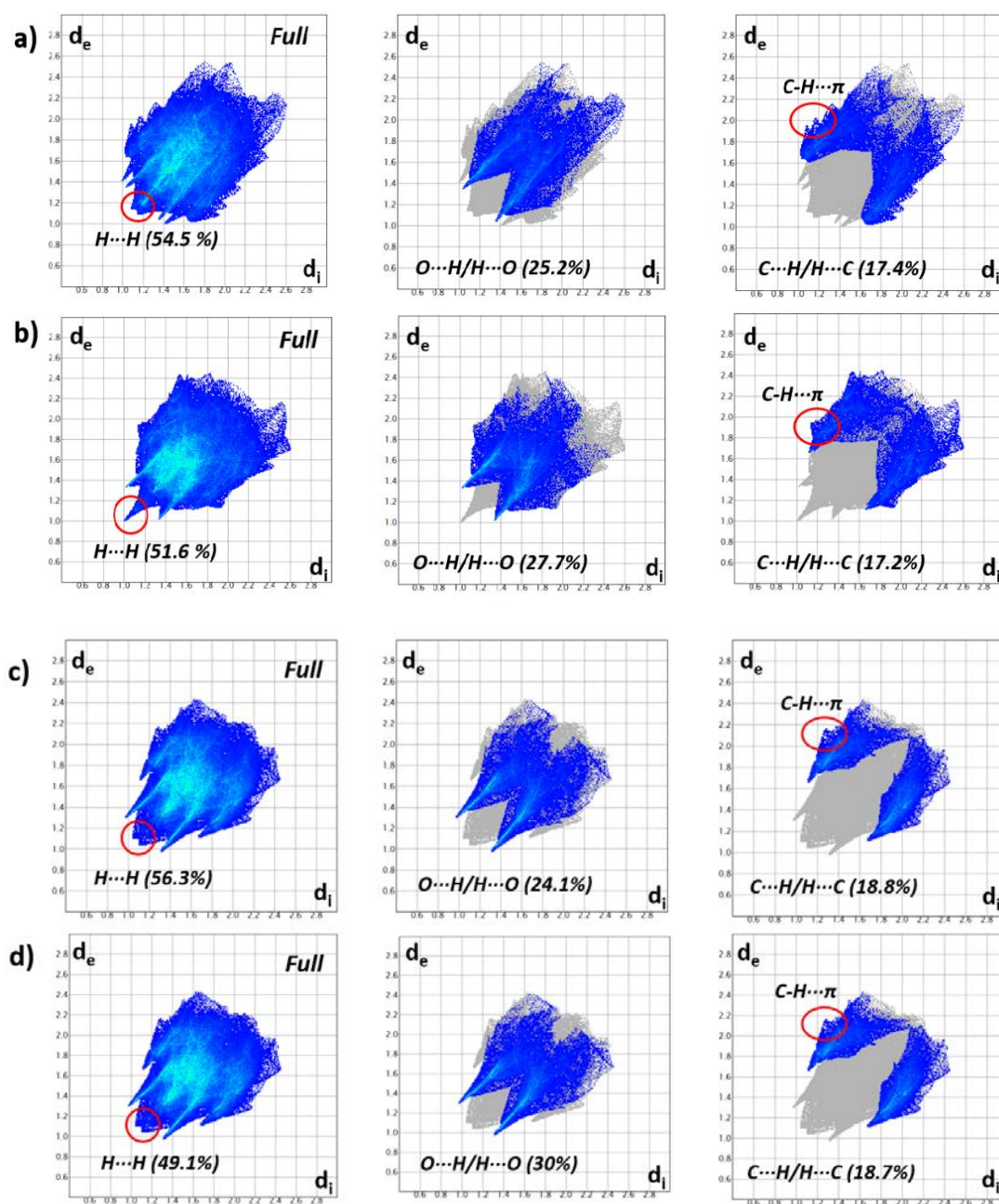
Figure 7. Full and decomposed 2D fingerprint plots for compounds: (**a**) **1**; (**b**) **2**; (**c**) **3** and (**d**) **4**.

The vdW forces (H⋯H contacts) have the largest contribution to the HS, and they are highlighted in the scattered middle points in the fingerprint plots with a minimum value of $(d_e + d_1) \sim 2.2$ Å (Figure 7), which is the sum of the vdW radii. All red areas that are visible on the surfaces mapped over d_{norm} function correspond to C–H⋯O contacts. For (**1**), the largest bright-red spot labeled 1 on the HS shows O⋯H/H⋯O contact associated with C17–H17C⋯O1 interaction, which constitutes the strongest among all interactions present in this compound. Two medium sized red spots labeled as 2 and 3 are associated with C15–H15A⋯O1 and C27–H27C⋯O4, respectively. These interactions are also visible as symmetrical sharp spikes centered at $(d_e + d_i) \cong 2.4$ Å in the fingerprint plots (Figure 7a) with 25.2% contribution to the Hirshfeld contact surface. The intermolecular C25–H25A⋯N1 contact is visible in the HS as a red spot labelled 4, which comprises 2.3% of the total HS area. The HS of (**2**) mapped over d_{norm} function (see Figure 6) shows four red spots, indicating the presence of C–H⋯O hydrogen bonds

[C13–H13A⋯O1 (**1**), C26–H16A⋯O4 (**2**), C10–H10B⋯O1 (**3**), C14–H14A⋯O2 (**4**)]. The decomposed fingerprint plots (Figure 7b) show that intermolecular O⋯H/H⋯O contacts contribute 27.7% to the total HS area. The O⋯H/H⋯O contacts appeared as sharp spikes with (de + di) ≅ 2.35 Å. In the HS of (**3**), the O⋯H/H⋯O contacts (Figure 6) are visible as six red spots attributed to C6–H6A⋯O3 (labeled 1), C10–H10B⋯O3 (labeled 1), C15–H15A⋯O4 (labeled 2) and C17–H17C⋯O4 (labeled 2). These interactions comprise the 24.1% of the HS area. A similar behavior was observed in the HS mapped over d_{norm} function for (**4**), which the six red spots observed (Figure 6) are attributed to C26–H26⋯O4 (1), C16–H16⋯O4 (2), C24,H24⋯O2 (3), C12–12⋯O3 (4) and C6–H6A⋯O3 (5). Intermolecular interactions O⋯H/H⋯O are observed around 2.3 Å which is slightly shorter than those of other compounds with 30% contribution to the Hirshfeld contact surface.

As was described previously, the structure of (**1**) is also stabilized by C–H⋯π interactions. The red area labeled 5 in the HS mapped over d_{norm} is attributed to C9–H9B⋯π. These C–H⋯π interactions are also evident from a pair of "wings" in the top left and bottom right region of the fingerprint plots for compounds **1**–**4** (Figure 7). The shape of the wings and the sum of d_e and d_i show the importance of this interaction. The decomposition of the fingerprint plots shows that the C⋯H/H⋯C contributions comprising 17.4%, 17.2%, 18.8% and 18.7% of the total HS for each molecule of **1**, **2**, **3** and **4**, respectively.

3.3. DFT Calculations

The DFT study is focused to analyze the supramolecular assemblies commented above in Figures 2–5, where combinations of C–H⋯π and C–H⋯O H-bonding networks are commonly formed in compounds **1**–**4**. First of all, the molecular electrostatic potential (MEP) surfaces of compounds **1** and **2** have been computed in order to analyze the electron rich and electron poor regions of the molecules. The surfaces are represented in Figure 8 and it can be observed that the most negative regions correspond to the O-atoms of the sulfonamide group. The N-atoms of the triazinane ring are not good H-bond acceptors, likely because either the lone pair is delocalized into the SO$_2$-group, in accordance with the S2–N5 and S1-N3 bond lengths of 1.632(1) and 1.642(1) Å, respectively indicating a double bond character of these bonds. The most positive region corresponds to the middle of the three axial H-atoms of the triazinane ring (+27 kcal/mol). The aromatic H-atoms and the CH$_3$ substituents also present positive MEP values (+23 and +20 kcal/mol, respectively). Finally, the MEP value over the aromatic rings is negative (−8 kcal/mol), thus adequate for establishing C–H⋯π interactions. The MEP analysis evidences that the most favored interactions from an electrostatic point of view are those involving the O-atoms as electron donors and either aromatic or triazinane protons as electron acceptors.
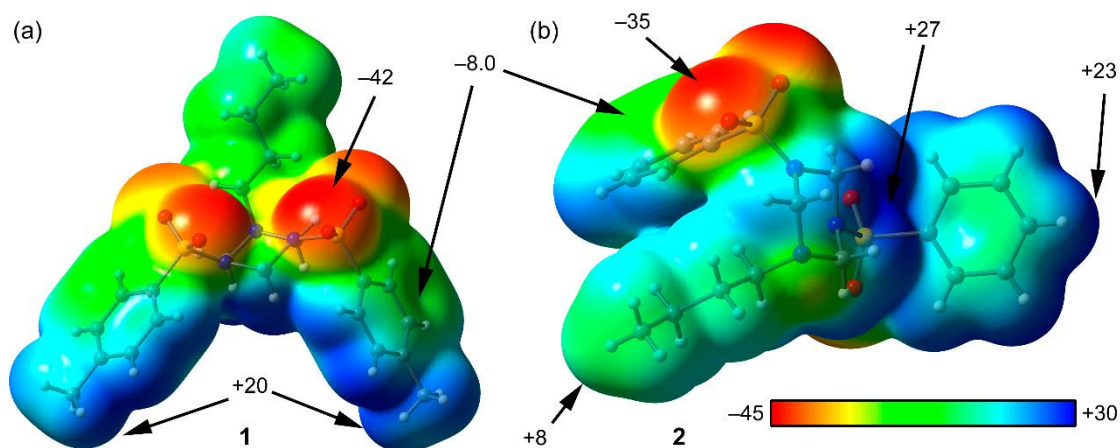

Figure 8. MEP surfaces for compounds **1** (**a**) and **2** (**b**). The energies at selected points of the surfaces are given in kcal/mol.

We have selected two supramolecular assemblies commented above in Figure 2 to analyze the energetic features of the H-bonds and C–H⋯π interactions in **1**. The QTAIM distribution of critical points and bond paths are also given in Figure 9. The existence of a bond CP and bond path connecting two atoms is a good indicator of interaction [21]. For the self-assembled dimer (Figure 9a), in addition to the symmetrically related H-bonds (characterized by a bond CP (critical point) and bond path interconnecting the H and O-atoms), the QTAIM analysis reveals the existence of a π⋯π stacking interaction that further stabilizes the formation of the dimer. The dimerization energy is moderately strong ($\Delta E_1 = -9.1$ kcal/mol) due to the contribution of both H-bonds and the π-stacking. We have also analyzed the other motif, where C–H⋯π interactions are established. The interaction energy is very strong ($\Delta E_2 = -20.4$ kcal/mol), because in addition to the C–H⋯π contacts (two bond CPs and bond paths connect two aromatic H-atoms to two carbon atoms of the adjacent ring) an intricate network of H-bonds is established where six C–H⋯O and one C–H⋯N contacts are formed, which are highlighted in Figure 9b by yellow circles.
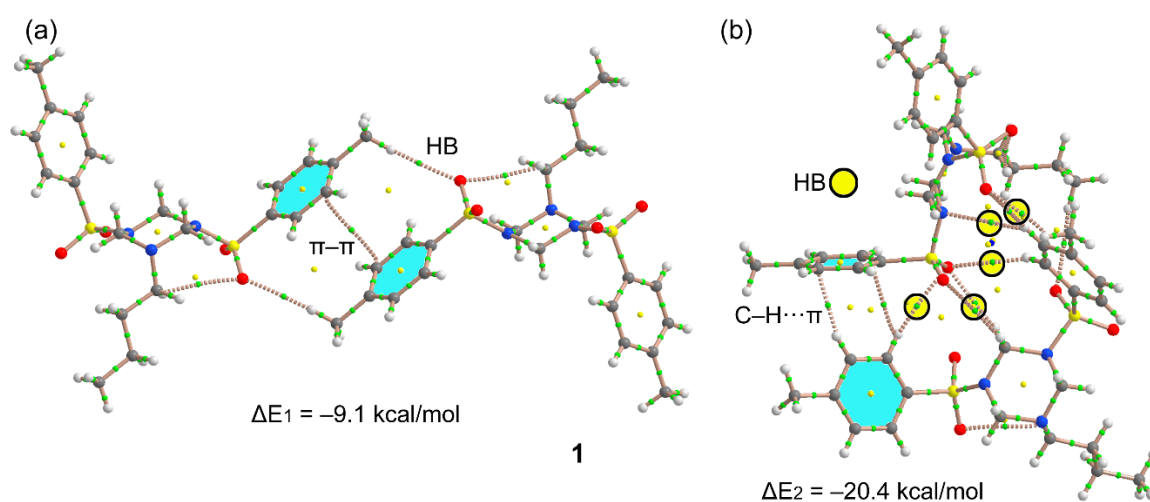
Figure 9. (**a**,**b**) Distribution of bond, ring and cage critical points (green, yellow and blue spheres, respectively) and bond paths in two dimers of complex **1**. The C–H⋯O bonds are highlighted in (**b**).

Figure 10a shows the self-assembled dimer of compound 2 where up to eight C–H⋯O contacts are established between either aromatic or aliphatic H-atoms and the O-atoms of sulfonamide (each one characterized by a bond CP and bond path, see yellow circles in Figure 10a). Moreover, two symmetrically distributed C–H⋯π interactions are also present and characterized by a bond CP and bond path connecting the aliphatic H-atom to one C-atom of the aromatic ring. As a consequence of this combination of interactions, the dimerization energy is very large $\Delta E_3 = -16.7$ kcal/mol, thus confirming the importance of this motif in the solid state of compound **2**. Figure 10b shows a dimer extracted from the infinite 1D chain represented in Figure 3b. In this case, the interaction energy is modest ($\Delta E_4 = -3.4$ kcal/mol) because only one H-bond is established. The distribution of bond CPs and bond path also reveals the existence of van der Waals interactions between the alkyl chain and the aromatic ring.

Figure 11 shows two dimers of compound **3**, one corresponds to the C–H⋯π assembly commented above in Figure 4, where in addition to the C–H⋯π interaction (characterized by a bond CP and bond path) the assembly is further characterized by a C–H⋯O bond involving the methyl group. This assembly presents a modest interaction energy of $\Delta E_4 = -5.9$ kcal/mol. In contrast, the dimer shown in Figure 11b, extracted from the infinite 1D assembly, exhibits a strong interaction energy ($\Delta E_5 = -17.3$ kcal/mol) due to the formation of four C–H⋯O contacts, which are characterized by a bond CP and bond path (see yellow circles in Figure 11b). The strong interaction energy agrees well with the MEP surface analysis commented above, since the H-bond donors belong to the triazinane

ring that exhibit the most positive MEP values. Moreover, the H-bond acceptors are the O-atoms of the sulfonamide groups that present the most negative MEP values (see Figure 8).
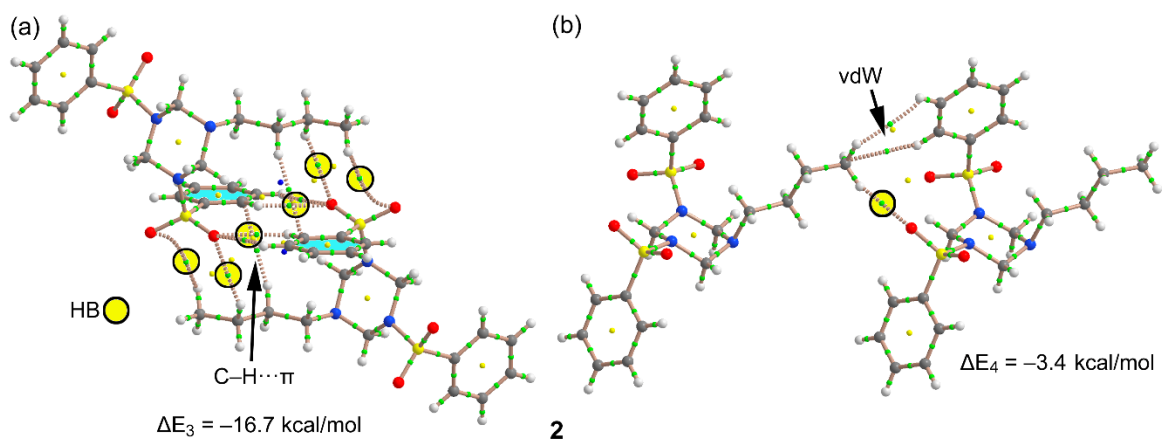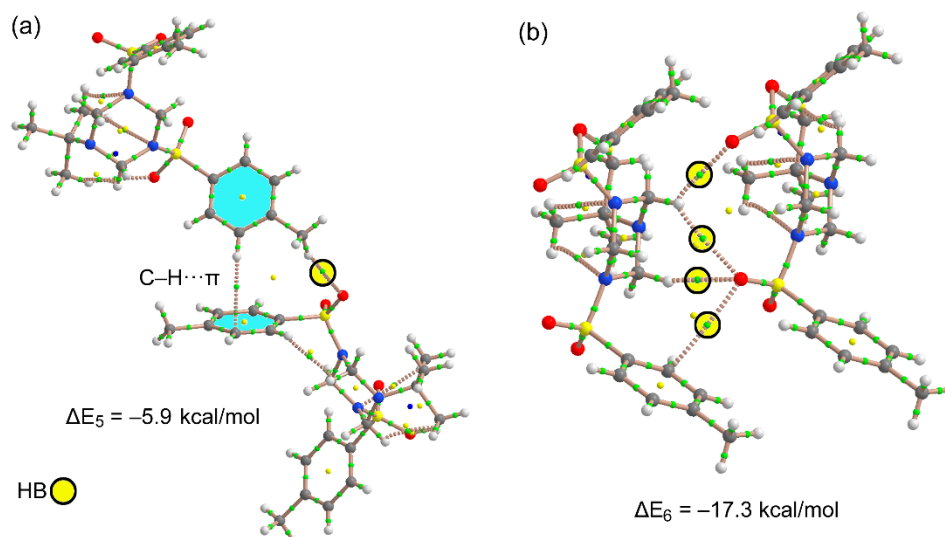

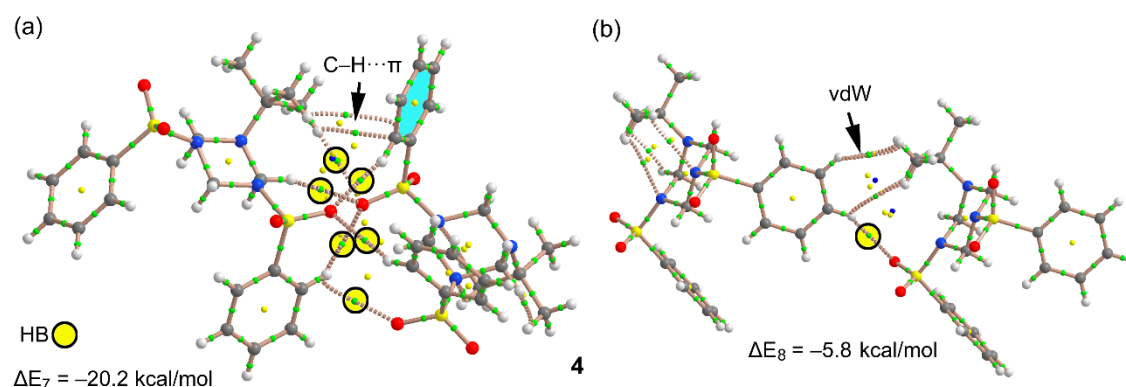**Figure 10.** (**a**,**b**) Distribution of bond, ring and cage critical points (green, yellow and blue spheres, respectively) and bond paths in two dimers of complex **2**. The C–H⋯O bonds are highlighted.

Figure 11. (**a**,**b**) Distribution of bond, ring and cage critical points (green, yellow and blue spheres, respectively) and bond paths in two dimers of complex **3**. The C–H⋯O bonds are highlighted.

Finally, Figure 12 shows the dimeric motifs analyzed in compound **4**. The dimer of Figure 12a presents an intricate combination of C–H⋯O bonds in addition to two C–H⋯π interactions involving the t-butyl group. As a consequence of the formation of six concurrent H-bonds, the dimerization energy is very large, $\Delta E_7 = -20.2$ kcal/mol. Figure 12b shows the dimer extracted from the 1D supramolecular polymer (see Figure 5b), which presents a modest interaction energy due to the formation of a single H-bond along with van der Waals contacts between the aromatic and aliphatic C–H bonds.

Figure 12. (**a**,**b**) Distribution of bond, ring and cage critical points (green, yellow and blue spheres, respectively) and bond paths in two dimers of complex **4**. The C–H⋯O bonds are highlighted.

4. Concluding Remarks

In summary, the synthesis and single crystal X-ray diffraction characterization of four N-substituted 1,3,5-triazinanes are reported along with a detailed analysis of the noncovalent interactions observed in the solid state. All complexes have in common the formation of several motifs characterized by a network of C–H⋯O interactions that exhibits very strong binding energies as a consequence of these cooperative H-bonds. Moreover, several structures also form interesting C–H⋯π⋯H–C ternary assemblies that have been described in detail. Besides, the MEP surfaces have been used to rationalize the noncovalent interactions and the QTAIM method to confirm the existence of the intricate combinations of H-bonds. Finally, the Hirshfeld surface analysis provides further evidence for the importance of C–H⋯π and C–H⋯O in the crystal packing of compounds **1**–**4**. We assume, that observed case of intramolecular sp^2-sp^3 disequalization makes the corresponding family of *N*-alkyl-*N′*,*N″*-substituted triazinanes an interesting object for research in the domain of local molecular disorder in organic crystals [25].

References

1. Ha, H.-J.; Koo Lee, W. Synthetic applications of Lewis acid-induced *N*-methyleneamine equivalents. *Heterocycles* **2002**, *57*, 1525–1538. [CrossRef]

2. Ji, D.; Sun, J. [3+2]-Cycloaddition of azaoxyallyl cations with hexahydro-1,3,5-triazines: Access to 4-imidazolidinones. *Org. Lett.* **2018**, *20*, 2745–2748. [CrossRef]

3. Ji, D.; Wang, C.; Sun, J. Asymmetric [4+2]-cycloaddition of copper–allenylidenes with hexahydro-1,3,5-triazines: access to chiral tetrahydroquinazolines. *Org. Lett.* **2018**, *20*, 3710–3713. [CrossRef]

4. Chen, L.; Liu, K.; Sun, J. Catalyst-free synthesis of tetrahydropyrimidines via formal [3+3]-cycloaddition of imines with 1,3,5-hexahydro-1,3,5-triazines. *RSC Adv.* **2018**, *8*, 5532–5535. [CrossRef]

5. Zhu, C.; Xu, G.; Sun, J. Gold-catalyzed formal [4 + 1]/[4 + 3] cycloadditions of diazo esters with triazines. *Angew. Chem. Int. Ed.* **2016**, *55*, 11867–11871. [CrossRef]

6. Liu, S.; Yang, P.; Peng, S.; Zhu, C.; Cao, S.; Li, J.; Sun, J. Gold-catalyzed sequential annulations towards 3,4-fused bi/tri-cyclic furans involving a [3 + 2 + 2]-cycloaddition. *Chem. Commun.* **2017**, *53*, 1152–1155. [CrossRef]

7. Liu, P.; Xu, G.; Sun, J. Metal-free [2 + 1 + 2]-cycloaddition of tosylhydrazones with hexahydro-1,3,5-triazines to form imidazolidines. *Org. Lett.* **2017**, *19*, 1858–1861. [CrossRef]

8. Peng, S.; Ji, D.; Sun, J. Gold-catalyzed [2 + 2 + 2 + 2]-annulation of 1,3,5-hexahydro-1,3,5-triazines with alkoxyallenes. *Chem. Commun.* **2017**, *53*, 12770–12773. [CrossRef]

9. Zeng, Z.; Jin, H.; Song, X.; Wang, Q.; Rudolph, M.; Rominger, F.; Hashmi, A.S.K. Gold-catalyzed intermolecular cyclocarboamination of ynamides with 1,3,5-triazinanes: En route to tetrahydropyrimidines. *Chem. Commun.* **2017**, *53*, 4304–4307. [CrossRef]

10. Garve, L.K.B.; Jones, P.G.; Werz, D.B. Ring-opening 1-amino-3-aminomethylation of donor-acceptor cyclopropanes *via* 1,3-diazepanes. *Angew. Chem. Int. Ed.* **2017**, *56*, 9226–9230. [CrossRef]

11. Yin, B. Synergistic Antimicrobial Composition. WO Patent 2,011,049,761, 28 April 2011.

12. Kletskov, A.V.; Frontera, A.; Sinelshchikova, A.A.; Grigoriev, M.S.; Zaytsev, V.P.; Grudova, M.V.; Bunev, A.S.; Presnukhina, S.; Shetnev, A.; Zubkov, F.I. Straightforward three-component synthesis of *N*-alkyl-*N′*,*N″*-substituted hexahydro-1,3,5-triazines. *Synlett* **2020**. [CrossRef]

13. Spackman, M.A.; Jayatilaka, D. Hirshfeld surface analysis. *CrystEngComm* **2009**, *11*, 19–32. [CrossRef]

14. McKinnon, J.J.; Spackman, M.A.; Mitchell, A.S. Novel tools for visualizing and exploring intermolecular interactions in molecular crystals. *Acta Cryst. B* **2004**, *60*, 627–668. [CrossRef]

15. McKinnon, J.J.; Jayatilaka, D.; Spackman, M.A. Towards quantitative analysis of intermolecular interactions with Hirshfeld surfaces. *Chem. Commun.* **2007**, 3814–3816. [CrossRef]

16. Spackman, M.A.; McKinnon, J.J. Fingerprinting intermolecular interactions in molecular crystals. *CrystEngComm* **2002**, *4*, 378–392. [CrossRef]

17. Turner, M.J.; McKinnon, J.J.; Wolf, S.K.; Grimwood, D.J.; Spackman, P.R.; Jayatilaka, D.; Spackman, M.A. *CrystalExplorer17*; University of Western Australia: Perth, Australia, 2017.

18. Frisch, M.J.; Trucks, G.W.; Schlegel, H.B.; Scuseria, G.E.; Robb, M.A.; Cheeseman, J.R.; Scalmani, G.; Barone, V.; Petersson, G.A.; Nakatsuji, H.; et al. *Gaussian 16, Revision A.01*; Gaussian, Inc.: Wallingford, CT, USA, 2016.

19. Bader, R.F.W. A quantum theory of molecular structure and its applications. *Chem. Rev.* **1991**, *91*, 893–928. [CrossRef]

20. Keith, T.A. *AIMAll (Version 13.05.06)*; TK Gristmill Software: Overland Park, KS, USA, 2013.

21. Bader, R.F.W. A Bond Path: A Universal Indicator of Bonded Interactions. *J. Phys. Chem. A* **1998**, *102*, 7314–7323. [CrossRef]

22. Breneman, C.M.; Weber, L.W. Charge and Energy Redistribution in Sulfonamides Undergoing Conformational Changes. Hybridization as a Controlling Influence over Conformer Stability. *Can. J. Chem.* **1996**, *74*, 1271–1282. [CrossRef]

23. Wilson, A.J.C.; Geist, V. International Tables for Crystallography. Volume C: Mathematical, Physical and Chemical Tables (See, Table 9.5.1.1.). *Cryst. Res. Technol.* **1993**, *28*, 110. [CrossRef]

24. Caine, B.A.; Bronzato, M.; Popelier, P.L.A. Experiment Stands Corrected: Accurate Prediction of the Aqueous pKa Values of Sulfonamide Drugs Using Equilibrium Bond Lengths. *Chem. Sci.* **2019**, *10*, 6368–6381. [CrossRef]

25. Habgood, M.; Grau-Crespo, R.; Price, S.L. Substitutional and Orientational Disorder in Organic Crystals: A Symmetry-Adapted Ensemble Model. *Phys. Chem. Chem. Phys.* **2011**, *13*, 9590. [CrossRef]